Received: 17 August 2021 | Revised: 12 January 2022 | Accepted: 13 January 2022

DOI: 10.1002/asl.1079

RESEARCH ARTICLE

Atmospheric Science Letters RMetS

Orographic enhancement of rainfall over the Congo Basin

Ajay Raghavendra[1] | Geng Xia[2] | Liming Zhou[3] | Yan Jiang[3]

[1]U.S. Army, Latham, New York, USA

[2]National Wind Technology Center, National Renewable Energy Laboratory, Golden, Colorado, USA

[3]Department of Atmospheric and Environmental Sciences, University at Albany, Albany, New York, USA

Correspondence
Ajay Raghavendra, U.S. Army, Latham, NY, USA.
Email: drajayraghavendra@gmail.com

Funding information
U.S. National Science Foundation, Grant/Award Numbers: AGS-1535426, AGS-1854486; National Renewable Energy Laboratory, operated by Alliance for Sustainable Energy, LLC; U.S. Department of Energy, Grant/Award Number: DE-AC36-08GO28308; U.S. Department of Energy Office of Energy Efficiency; Renewable Energy Wind Energy Technologies Office

Abstract

The Congo rainforest located in central equatorial Africa is an important, yet understudied part of the globe surrounded by complex orographic features. A primitive understanding of precipitation processes such as mesoscale convective dynamics magnifies uncertainties in the future climate projections of the hydrological cycle over the Congo. Furthermore, the effects of orography, which is an important forcing for convection and precipitation, are poorly resolved by climate models, and ill-conceptualized over the Congo. To address this knowledge gap, perturbed orographic forcing experiments are conducted using the Weather Research and Forecasting (WRF) mesoscale numerical model in a high-resolution convection-permitting model setup. The model simulated selected dates in November 2014. The thunderstorms and rainfall simulated in the control run for the case study analyzed in this article compared reasonably well to satellite-derived brightness temperature and rainfall data. The results from this case study show that the dynamical impact of increasing the height of the East African Highlands is the blocking of the lower-tropospheric tropical easterlies. This weakening of the lower-tropospheric zonal winds increases the windshear over the Congo Basin resulting in slower propagating, more intense mesoscale convective systems with enhanced rainfall.

KEYWORDS

Congo rainforest, orographic forcing, tropical convection, WRF model

1 | INTRODUCTION

The second largest and one of the most understudied rainforests of the world, that is, the Congo located in equatorial Africa is also the driest (rainfall totaling ~1500 mm year^{-1}) when compared to other major rainforests (Zhou *et al.*, 2014; Alsdorf *et al.*, 2016). The Congo rainforest exists despite the significantly lower rainfall amount, is an important influence in the global carbon cycle, and particularly vulnerable to climate change (Haensler *et al.*, 2013; Malhi *et al.*, 2013). Unfortunately, the general circulation models (GCMs) used in the Coupled Model Intercomparison Project Phase 5 (CMIP5; Taylor *et al.*, 2012) produce a large spread in the historic and future climate projections of precipitation over the Congo basin (Haensler *et al.*, 2013; Washington *et al.*, 2013). Some of these uncertainties may be attributable to the coarse representation of orography (Figure 1) and mesoscale convective dynamics (Dai, 2006; Chen & Dai, 2019) in low-resolution datasets.

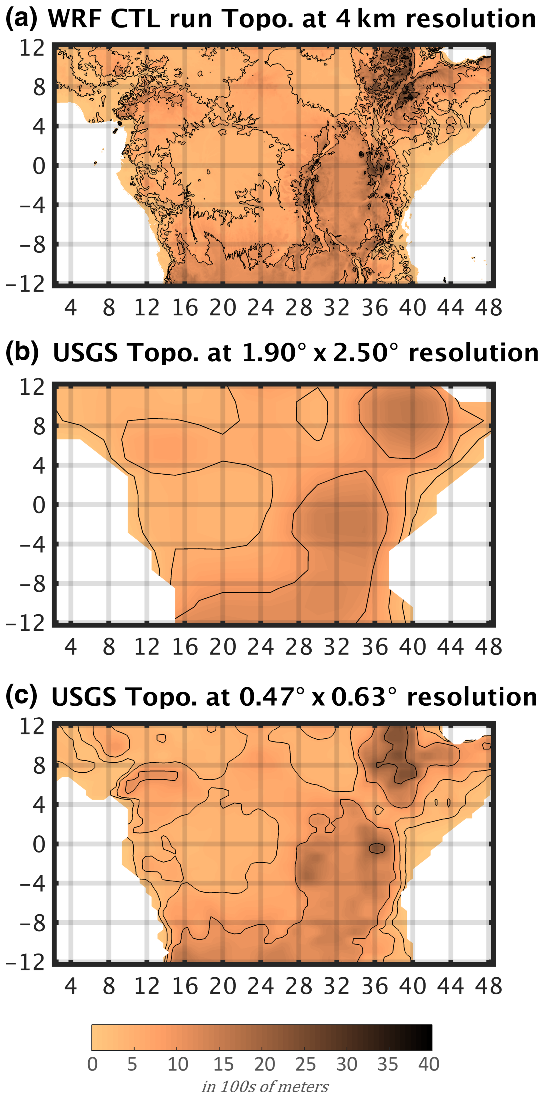

FIGURE 1 Topographical input data used in the (a) WRF CTL run presented in this study, (b) a typical GCM (e.g., CMIP5 models), and (c) a higher-resolution GCM

Over the Congo, there is still considerable debate on what role topographical features such as the Ethiopian highlands, Turkana channel, and East African Highlands play in channeling moisture into the Congo (Dyer *et al.*, 2017; Sorí *et al.*, 2017), and whether these orographic features surrounding the Congo work to enhance or suppress thunderstorm activity and rainfall. From a dynamic perspective, orography plays a profound role as an atmospheric forcing. For instance, atmospheric flow over a mountain may result in atmospheric wave activity, flow blocking, cyclogenesis (lee cyclogenesis, e.g., Pontoppidan *et al.*, 2019), and precipitation enhancement or suppression (Sotillo *et al.*, 2003). The persistent easterly low-level jet and associated moisture transport over the African highlands (King *et al.*, 2021; Munday *et al.*, 2021) further motivates the investigation of orographic enhancement of rainfall over the Congo. Other factors that encourage the study of orography include micrometeorological constraints such as sunlight availability for photosynthesis and evapotranspiration over mountainous regions (Motzer, 2005; Crowhurst *et al.*, 2021).

The Congo basin is often regarded as a “convective engine” of the global atmospheric circulation and is the world's foremost lightning hotspot (Malhi *et al.*, 2013). Furthermore, mesoscale convective systems (MCSs) are the primary source for rainfall across tropical Africa (Jackson *et al.*, 2009; Taylor *et al.*, 2018). While large scale influences of Africa's orography have been investigated to understand the south east Asian Monsoon (Wie and Bordoni, 2016), and the influence of the East African highlands on the atmospheric circulation, temperature, and rainfall over Africa have been evaluated using numerical models (Slingo *et al.*, 2005; Sommerfeld *et al.*, 2016), many unanswered questions pertaining to mechanisms for MCS activity and rainfall over the Congo persist. Jackson *et al.* (2009) inferred that the interannual variability in convection and MCS activity over the Congo Basin is dictated by changes in the interaction between wind speed and local topography over time. But the association between rainfall and topography was based on empirical analyses of satellite observations and reanalysis data, which cannot directly clarify causality. This article seeks to narrow the knowledge gap by establishing a clearer understanding of the role that African orography plays in modulating thunderstorm activity and rainfall over the Congo. In this study, a high-resolution convection-permitting mesoscale numerical modeling framework is invoked. Since orography is the only perturbed field in such an experiment, changes in the atmosphere, thunderstorms, and rainfall characteristics may be predominantly attributable to orographic changes (Rasmussen and Houze, 2016).

2 | MODEL SETUP

Geostationary infrared (IR) 11 μm channel brightness temperature (T_b) data derived from GridSat-B1 satellite data (Knapp, 2008; Knapp *et al.*, 2011) show that MCSs were present on November 5, 2014 with a particularly large spatial extent over the Congo Basin, i.e., observations (OBS) in Figure, that contained both large and small convective cells characterized by cold cloud top temperatures. Intense tropical thunderstorms are generally characterized by colder cloud top temperatures, and vice versa (Raghavendra *et al.*, 2018). This event was selected as the case study in the paper as it is a typical

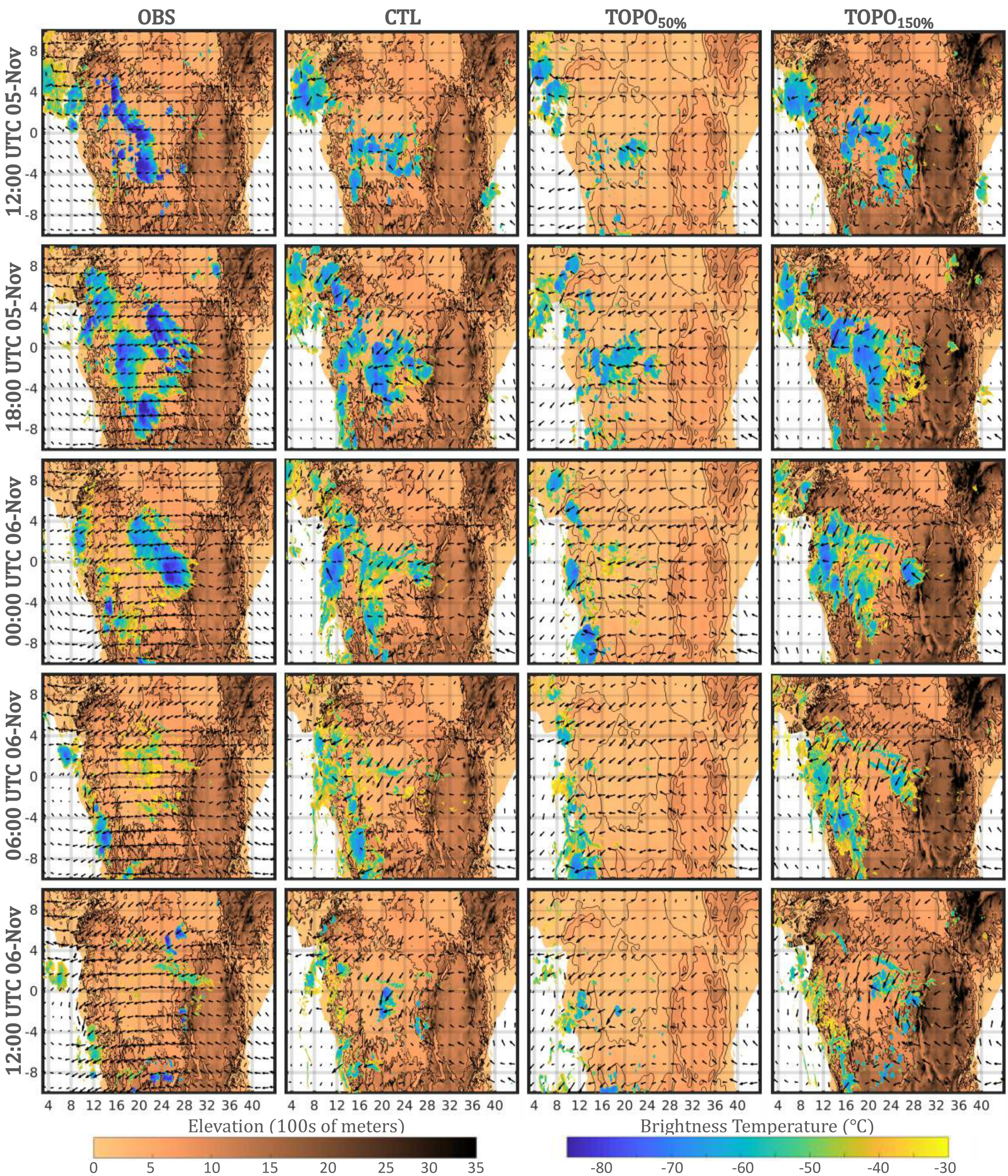

FIGURE 2 The evolution of MCSs diagnosed using cold cloud top brightness temperature (T_b) over equatorial Africa shown every 6 h from 1200 UTC on November 5 to 1200 UTC on November 6, 2014, from GridSat-B1 (OBS), and CTL, $TOPO_{50\%}$, and $TOPO_{150\%}$ runs. Zonal and meridional wind vectors from ERA-I (800–500 hPa layer mean for OBS) and the WRF model (2–5 km layer mean) are also displayed. Color bars for orography (in 10^2 m) and T_b (in °C) are displayed below the figure

representation of MCS activity over the basin in November, which is the month with the strongest relationship between lower tropospheric easterlies and thunderstorm activity over the Congo. The data show that a few isolated and relatively weak thunderstorm cells (with relatively warm cloud top temperatures) propagated westward over the East African Highlands and entered the lowlands of the Congo basin between 0000–0600 UTC on November 5 (available through the global international satellite cloud climatology project (ISCCP) B1 browse system, i.e., GIBBS, archive). Once over the Congo basin, these thunderstorm cells organized to form a large, quasilinear shaped MCS between 1200 and 1800 UTC. On November 6, between the hours of 0300 and 1200 UTC, the MCS was observed to dissipate.

The NCAR Weather Research and Forecasting (WRF) Advanced Research WRF (WRF-ARW) model version 3.6.1 (Skamarock *et al.*, 2008) was tested to assess whether it was able to successfully capture this typical mesoscale convective event (Laing *et al.*, 2011). The model configuration for the simulations utilized the ARW-WRF version 3.6.1 run as a compressible, nonhydrostatic, and three-dimensional mesoscale model. The model was initialized with the European Centre for Medium-Range Weather Forecast (ECMWF) interim reanalysis (ERA-I; Dee *et al.*, 2011) data at 0000 UTC November 2, 2014, and ran continuously without spectral nudging for 120 hours (i.e., simulation ends on 0000 UTC November 7, 2014) using a large domain (1300 [latitude] × 700 [longitude] grid points) at 4 km horizontal resolution centered around the Congo basin (Figure 1a). The first 48 hours were reserved for model stabilization and spin-up, and a detailed evaluation of the simulations is presented from 1200 UTC November 5 to 1200 UTC November 6. The simulation used 38 vertical levels with the finest resolution in the planetary boundary layer (PBL) and incorporated the following parameterization schemes which closely follows Rasmussen and Houze (2016): Longwave Radiation: Rapid Radiative Transfer Model (Mlawer *et al.*, 1997), Shortwave Radiation: Dudhia (Dudhia, 1989), Surface Layer: Revised MMR surface layer scheme (Jiménez *et al.*, 2012), Microphysics: Thompson 6-class scheme with graupel and double moment for cloud ice (Thompson *et al.*, 2008), Land Surface: Noah Land Surface (Chen & Dudhia, 2001), and PBL: Yonsei University PBL (Hong *et al.*, 2006). Given the relatively high horizontal resolution, convection was explicitly resolved, and a cumulus parameterization scheme was not invoked.

Three simulations including the control run (CTL) were conducted using the ARW-WRF model. The CTL run followed the model setup previously described in this section and utilized the U.S. Geological Survey (USGS) topography and land classification. Two perturbation runs were setup in a manner identical to the CTL run with the exception of the input orography file. The model run with a 50% lower orography ($TOPO_{50\%}$) compared to the CTL was supplied with a modified topography file where the African orography was multiplied by 0.5 and smoothened once using 10 grid points in each direction. The result closely resembles the input orography file for a typical GCM (Figure 1b). On the other hand, the model run with a 50% higher orography ($TOPO_{150\%}$) compared to the CTL was supplied with a modified topography file where the African orography was multiplied by 1.5. The differences in the topographical input for the three model runs may be visualized in Figure 2.

3 | MODEL VALIDATION

The WRF-derived outgoing longwave radiation (OLR) data were converted to brightness temperature using the Stefan-Boltzmann law to enable the WRF model data to be evaluated for accuracy against the GridSat-B1 data. Studying the spatial patterns and temporal evolution of the MCSs observed by the GridSat-B1 data, and MCSs and rainfall simulated by the WRF model provides snapshots to validate the CTL run. Figure 2 shows the spatial extent and intensity of thunderstorm activity from the observations and three model runs for five timesteps. A qualitative analysis of the OBS and CTL images shows that the CTL run is able to reasonably reproduce the major features including the location, development, and propagation of thunderstorms from OBS. The NNW–SSE oriented quasi-linear squall line over the Congo at 1200 UTC on November 5 in the OBS is simulated with a WNW-ESE orientation in the CTL run. At 1800 UTC on November 5, however, the MCSs are reasonably well captured in the CTL run. A single organized thunderstorm cluster located near the eastern edges of the Congo at 0000 UTC on November 6 in the OBS is simulated as multiple scattered thunderstorm cells across the Congo in the CTL run. In both the OBS and CTL run, a significant reduction in thunderstorm activity is observed between 0000 and 0600 UTC. This activity remains low between 0600 and 1200 UTC on November 6. Some deviations from observations are expected in the CTL run since it is unrealistic to expect a model initialized and forced with a coarser resolution reanalysis data to reproduce observations without some degradation. Also, the WRF model is sensitivity to the choice of parameterization schemes, and spectral nudging which forces the WRF model output closer to the input data was not incorporated (Stratton *et al.*, 2018).

Hovmöller diagrams (Figure 3a–c,e–g) were constructed to further evaluate the CTL run against the satellite observations. Unlike the spatial comparison of thunderstorms in Figure 2, the Hovmöller diagram allows for the comparison of timing and propagation characteristics of thunderstorms between the OBS and CTL run. The primary MCS analyzed in this study is shown in the OBS and CTL run starting at 1200 UTC on

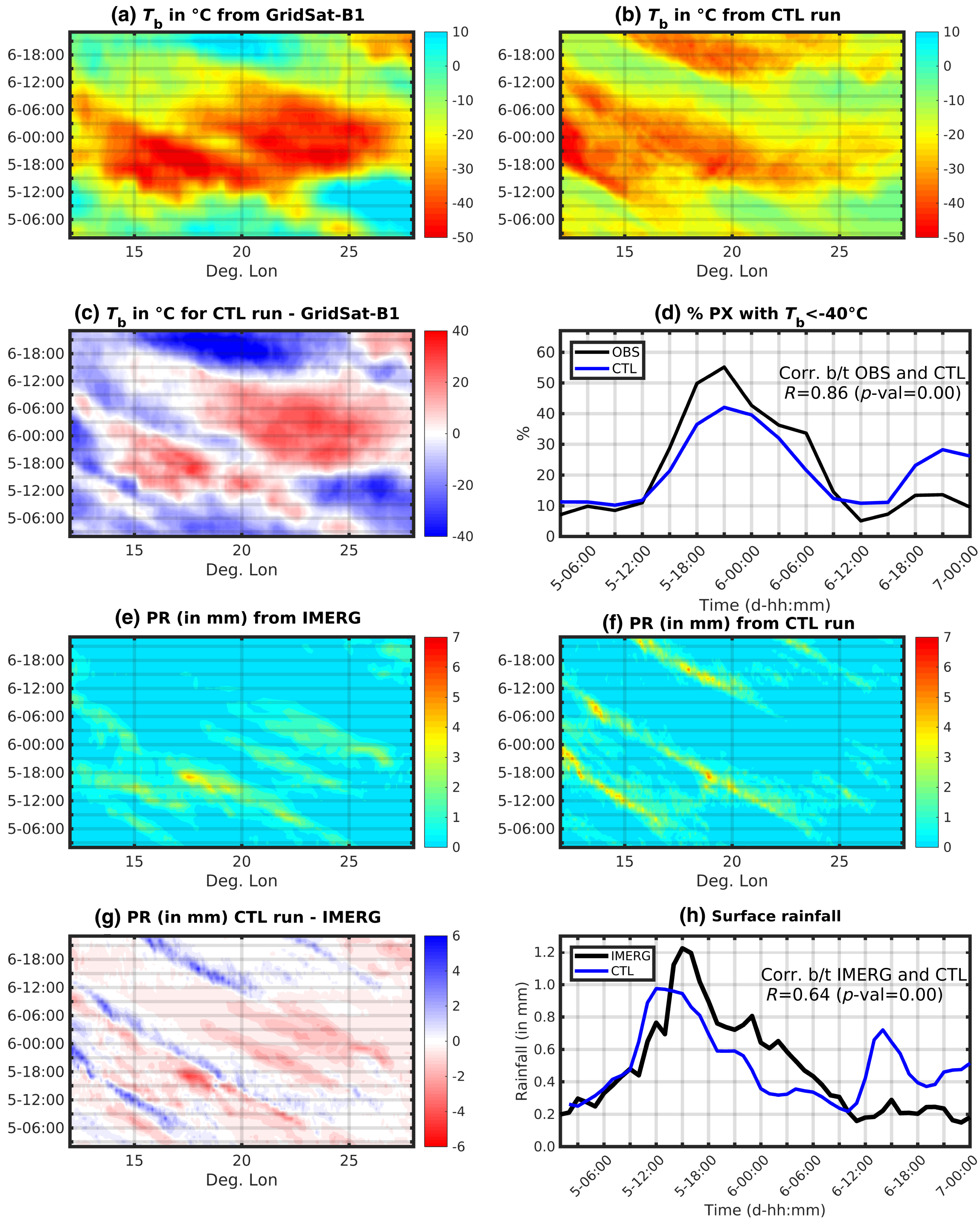

FIGURE 3 Hovmöller diagrams showing the longitude-time evolution of T_b from (a) GridSat-B1, (b) CTL run, and (c) CTL run–GridSat-B1. (d) Spatial extent of cold cloud pixels (PX) from the CTL run and GridSat-B1. Rainfall from (e) IMERG, (f) CTL run, and (g) CTL run–IMERG. (h) Spatially averaged hourly rainfall from the CTL run and IMERG. All data were spatially averaged between 5°N/S, and between 12° and 28° for (e)

November 5 near 22°E. The thunderstorm cells propagate westward and linearly in time starting from about 22°E to 12°E over a 24-hour period. The propagation characteristics of thunderstorms are similar between the OBS and CTL run, but some differences in the overall spatial structure of the thunderstorms are worth noting. In Figure 3c, regions shaded in blue show convective activity in the CTL run that are absent in the observations and vice-versa for regions shaded in red. Overall, there is a significantly correlation ($R = 0.86$) in the time evolution of cold cloud between the OBS and CTL over the Congo (Figure 3d). As in the OBS, the CTL run also reproduces the tropical diurnal cycle of thunderstorm activity over land (Figure 3d).

Due to the sparse surface observation network over the Congo (Washington *et al.*, 2013), calibrated precipitation estimates from the Integrated Multi-satellitE Retrievals for GPM (GPM IMERG Final Precipitation L3 Half Hourly $0.1^\circ \times 0.1^\circ$ V06; Huffman *et al.*, 2019a; 2019b) was also used for additional model validation (Figure 3e–h). The high-resolution IMERG dataset may be directly used to validate the WRF output with minimal interpolation errors. Given the strong relationship between convective activity and rainfall, the differences in rainfall between the OBS and CTL run closely follow the differences in the spatial extent of convective activity (Figure 3e–g). The time evolution of rainfall between the IMERG and CTL run was also significantly correlated ($R = 0.64$; Figure 3h). In summary, Figures 2 and 3 demonstrates that the WRF model performs reasonably well in capturing the MCSs which occurred between November 5 and 6, 2014. Additional methods to validate the model output with observations would be challenging over the Congo due to the lack of high-frequency surface or air/space-borne observations (Washington *et al.*, 2013; Alsdorf *et al.*, 2016), and the inability to properly resolve mesoscale events and precipitation characteristics even in the latest high-resolution reanalysis products such as ERA-5.

4 | RESULTS

The orographic impacts on the circulation, thunderstorm, and precipitation between the CTL, $TOPO_{50\%}$, and $TOPO_{150\%}$ runs are presented in this section. Results include the spatial extent and propagation characteristics of thunderstorm activity, rainfall, and the windfield structures. Differences in the vertical (height–longitude) cross sectional view of winds, specific humidity, and precipitation are also presented in this section.

4.1 | Spatial extent and intensity of thunderstorms and rainfall

Differences in the spatial extent of thunderstorms and their intensity between the three WRF model runs are illustrated in Figure 2. At all timesteps, the $TOPO_{50\%}$ run produces fewer and weaker thunderstorms, while the $TOPO_{150\%}$ run is characterized by stronger and more intense thunderstorms. While the overall location of the thunderstorm cells in the three WRF model runs are similar, the spatial extent and intensity of thunderstorms show considerable differences. At 1200 UTC and 1800 UTC on November 5, there are few differences in the spatial extent of thunderstorms between the CTL and $TOPO_{150\%}$ runs while the thunderstorms in the $TOPO_{50\%}$ run are considerably smaller. At 0000 UTC on November 6, most of the thunderstorms have moved away from the Congo basin and are located over the west-African coastline in the $TOPO_{50\%}$ run. At the same time, thunderstorms persist in the CTL and $TOPO_{150\%}$ runs. As typically observed for the tropical diurnal cycle over land, from 0000 UTC to 1200 UTC on November 6, thunderstorms dissipate overnight and through the morning hours.

Tropical thunderstorm intensity may be assessed using cold cloud top temperatures (Raghavendra *et al.*, 2018). The spatial extent, intensity, and propagation characteristics of thunderstorms in the CTL, $TOPO_{50\%}$, and $TOPO_{150\%}$ runs may be further analyzed using Hovmöller diagrams in Figure 4a–d and Figure 5a–d. As in Figure 2, the thunderstorms are large and more intense in the $TOPO_{150\%}$ run when compared to the $TOPO_{50\%}$ run. When compared to the CTL run, the spatial extent and intensity of thunderstorms in $TOPO_{50\%}$ run are smaller. The dominance of warmer red shading in Figure 4b shows that the thunderstorms in $TOPO_{50\%}$ run are not as intense when compared to their CTL run counterparts. On the other hand, Figure 4c,d shows that thunderstorms in the $TOPO_{150\%}$ run are larger and more intense when compared to their CTL counterparts. Finally, the spatial extent of cold cloud top pixels shows fewer cold clouds in the $TOPO_{50\%}$ when compared to the $TOPO_{150\%}$ run (Figure 4e).

Over the tropical latitudes, a strong relationship between convective activity and rainfall are expected (Dai, 2006). In order to evaluate convective activity and rainfall, surface rainfall data are presented in Figure 5. As expected, the spatial structure, intensity, and difference in rainfall between the experimental runs (i.e., $TOPO_{50\%}$ and $TOPO_{150\%}$ runs) and CTL run closely follow Figure 4. Figure 5b shows red streaks and Figure 5d shows blue streaks indicative of reduced rainfall in the $TOPO_{50\%}$ run and enhanced rainfall in the $TOPO_{150\%}$ run when compared to the CTL run. Figure 5f shows that the total accumulated rainfall over the Congo is largest for the $TOPO_{150\%}$ ($\sim$26 mm) and smallest for the $TOPO_{50\%}$ run ($\sim$13 mm).

4.2 | Vertical windshear

Vertical windshear is an important ingredient for the maintenance and longevity of an MCS (Chen *et al.*, 2015;

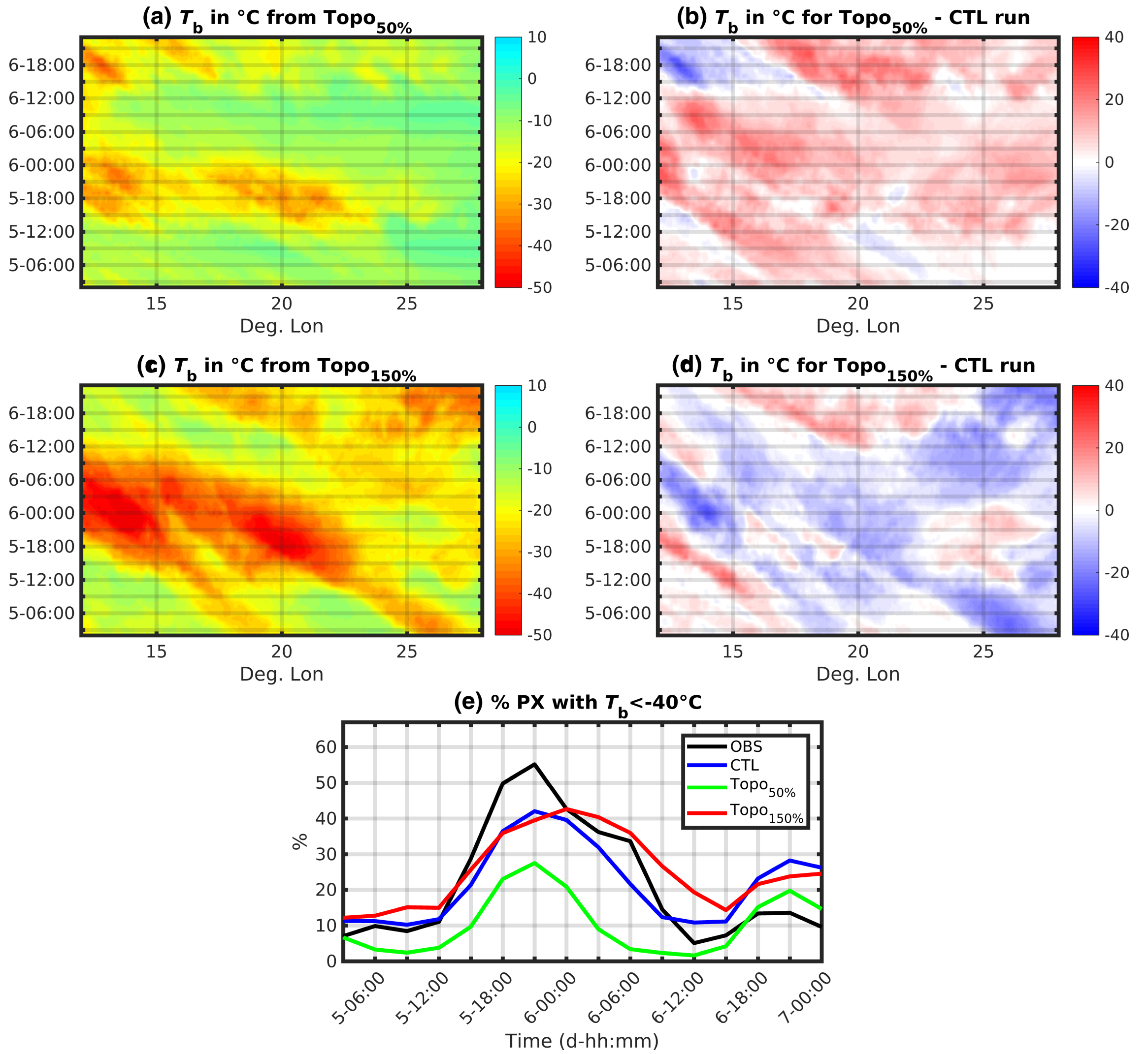

FIGURE 4 Hovmöller diagrams showing the longitude-time evolution of T_b from (a) TOPO$_{50\%}$ run, (b) TOPO$_{50\%}$–CTL run, (c) TOPO$_{150\%}$ run, and (d) TOPO$_{150\%}$–CTL run. (e) Spatially averaged T_b from GridSat-B1, CTL, TOPO$_{50\%}$, and TOPO$_{150\%}$ runs. All data were spatially averaged between 5°N/S, and between 12° and 28° for (e)

Taylor *et al.*, 2018). The time evolution of the mid- and lower-tropospheric horizontal winds are presented as a Hovmöller diagrams in Figure 6. In Figure 7, the zonal, meridional, and vertical windshear are analyzed quantitatively. The analysis is presented using geopotential height (km) instead of pressure-level (hPa) in order to contextualize the results against the background orography. The Hovmöller diagrams in Figure 6 show a similar overall structure for the 5.3 km (approximately 500 hPa) winds for all three model runs. The lower tropospheric winds at 1.2 km (approximately 850 hPa) on the other hand show large magnitude differences in the zonal winds and structural differences in the meridional winds. The strength of the lower-level zonal winds is strongest in the TOPO50% run, and weakest in the TOPO150% run. The zonal and meridional windshear is strongest in the TOPO$_{150\%}$ run when compared to the TOPO$_{50\%}$ run.

Orography blocks the easterly flow at the lower levels (~2 km), but has little impact in the mid-levels (~5 km). The blocking of the lower-level winds produces larger windshear in the TOPO1$_{50\%}$ run when compared to the TOPO$_{50\%}$ run. Figure 7 shows the basin-wide average zonal wind and meridional wind across the case study period at 5 and 2 km. In the mid-levels, there is very little difference in the zonal windspeed among the CTL, TOPO$_{50\%}$, and TOPO$_{150\%}$ runs (Figure 7a). In the lower-levels however (Figure 7b), the zonal winds hover between −8 and −10 ms^{-1} in the TOPO$_{50\%}$ run and between 0 and −4 ms^{-1} in the TOPO$_{150\%}$ run. Orography acts to drastically reduces the zonal windspeed and thus enhancing the vertical windshear. The mid- (Figure 7c)

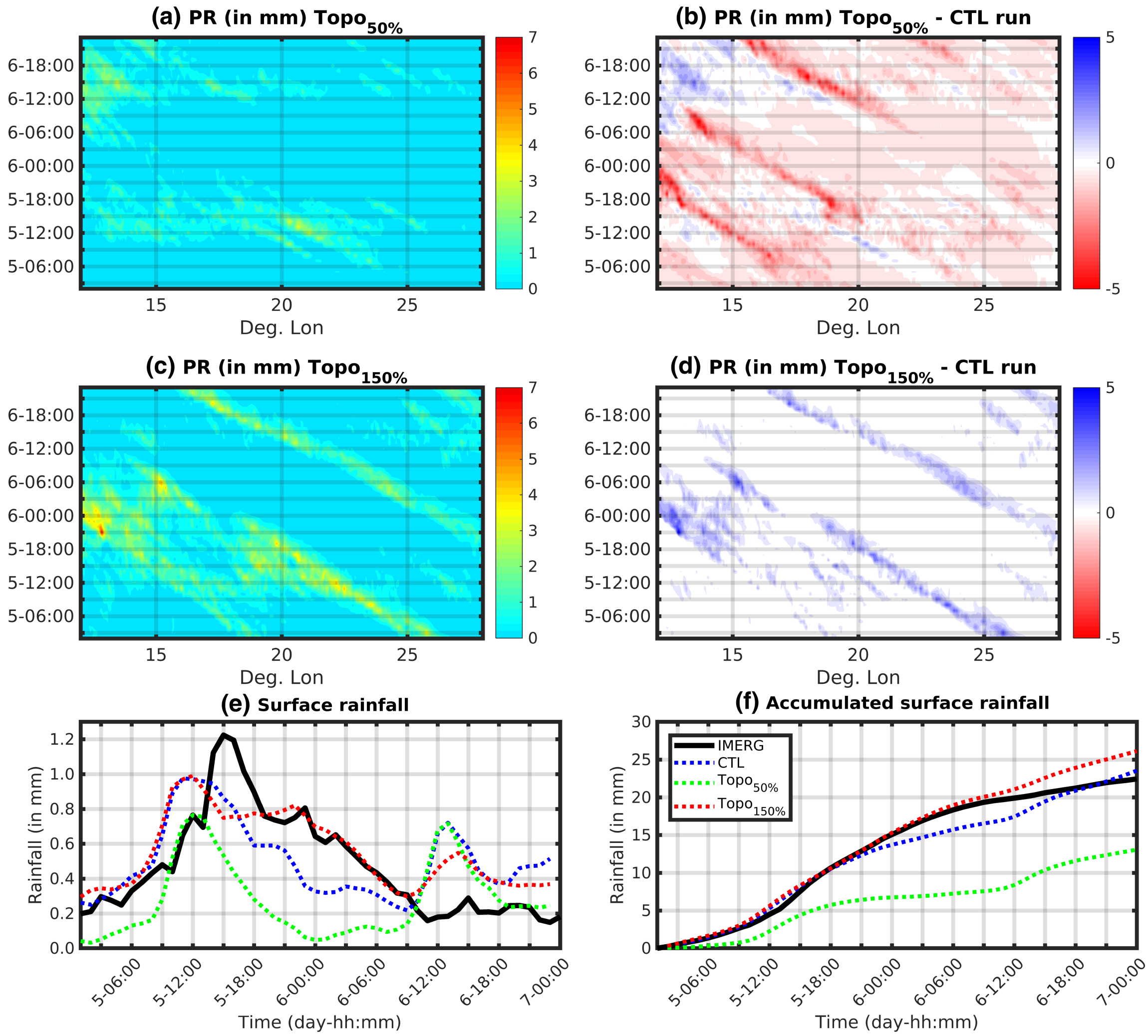

FIGURE 5 Hovmöller diagrams showing the longitude-time evolution of rainfall from (a) $\text{TOPO}_{50\%}$ run, (b) $\text{TOPO}_{50\%}$–CTL run, (c) $\text{TOPO}_{150\%}$ run, and (d) $\text{TOPO}_{150\%}$–CTL run. Spatially averaged (e) hourly and (f) accumulated rainfall from IMERG, CTL, $\text{TOPO}_{50\%}$, and $\text{TOPO}_{150\%}$ runs. All data were spatially averaged between 5°N/S, and between 12° and 28° for (e) and (f)

and lower- (Figure 7d) levels meridional winds do not show any substantial spread between the three model runs and are weaker when compared to their zonal wind counterparts.

For the period 1200 UTC November 5 to 1200 UTC November 6, the magnitude of the time mean zonal windshear for the $\text{TOPO}_{50\%}$ run is 1.0 ms^{-1}, and $\text{TOPO}_{150\%}$ run is 4.9 ms^{-1}. This result points to a mean increase of 3.9 ms^{-1} in the zonal windshear between the low and high orography runs (Figure 7a,b). On the other hand, the magnitudes of the time mean meridional windshear is 2.2 ms^{-1} for the $\text{TOPO}_{50\%}$ run and is 3.1 ms^{-1} $\text{TOPO}_{150\%}$ run. This results in a small increase in the mean meridional windshear by 0.9 ms^{-1} with higher orography (Figure 7c,d). At the mid-levels (solid line in Figure 7e), there is a narrow spread in the mean wind speed between the three runs and ranges between 7.7 and 8.0 ms^{-1}. However, the mean wind speed for the lower level (dashed line in Figure 7e) for the three runs shows a larger spread and ranges between 3.1 and 8.8 ms^{-1}. The $\text{TOPO}_{50\%}$ produces the weakest mean vertical windshear of -1.0 ms^{-1}, while the $\text{TOPO}_{150\%}$ run produces the strongest mean vertical windshear of 4.2 ms^{-1} (Figure 7f).

4.3 | Vertical cross-sectional analysis

Since the magnitude of the zonal wind is more than double when compared to the meridional wind, a longitude-height cross-sectional analysis by averaging 10 latitude points (40 km) across the equator for zonal and vertical winds, the rain/ice particle number concentration, and surface rainfall are presented in Figure 8. The most pronounced differences between the CTL, $\text{TOPO}_{50\%}$, and $\text{TOPO}_{150\%}$ runs are the intensity and diameter of the

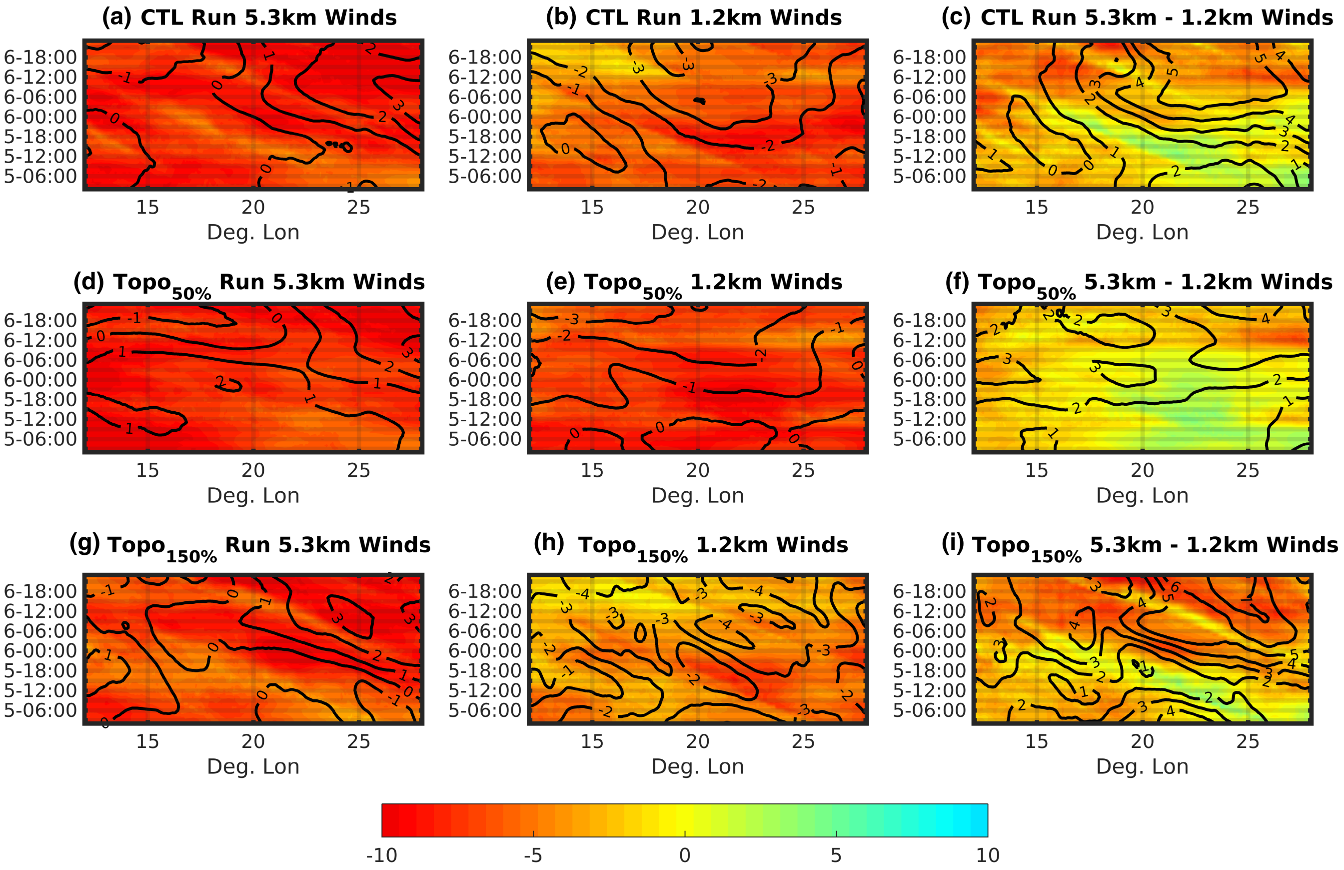

FIGURE 6 Hovmöller diagrams showing the longitude-time evolution of zonal (shaded; ms^{-1}) and meridional (contoured; ms^{-1}) winds from CTL run at (a) 5.3 km, (b) 1.2 km, and (c) 5.3–1.2 km windshear. (d–f) As in a–c but for the $TOPO_{50\%}$ run. (g–i) As in a–c but for the $TOPO_{150\%}$ run. All data were spatially averaged between 5°N/S

precipitation shaft, and the strength and propagation of the convective updrafts and downdrafts. The $TOPO_{150\%}$ run is characterized by a stronger and wider precipitation shaft, and consequently produces the largest surface rainfall amounts when compared to the $TOPO_{50\%}$ run. As shown in Section 4.2, the strong vertical windshear in the $TOPO_{150\%}$ run when compared to the $TOPO_{50\%}$ run may assist in the overall strength and longevity of these thunderstorms (Marion & Trapp, 2019). The enhanced MCS and rainfall in the $TOPO_{150\%}$ run when compared to the $TOPO_{50\%}$ run may also be attributable to the de-coupling of the thunderstorm updraft downdraft pair as a result of strong orographically forced vertical windshear. The strong vertical windshear delays the weakening of the updraft by the downdraft by decoupling of the thunderstorm updraft downdraft pair during the mature phases of the thunderstorm's lifecycle. Therefore, the lifecycle of the thunderstorm is prolonged and allows the thunderstorm to potentially evolve into a complex and well organized MCS (Marion & Trapp, 2019).

These intense thunderstorm cells in the $TOPO_{150\%}$ run also produces higher rainfall amounts while the $TOPO_{50\%}$ run produces lesser rainfall (Figure 5). Reinforcing the larger rainfall amounts in the $TOPO_{150\%}$ run is the slower propagation speed of the rain shaft when compared to the $TOPO_{50\%}$ run. The lower rainfall in the $TOPO_{50\%}$ run leads in time, whereas the higher rainfall in the $TOPO_{150\%}$ run lags in time when compared to the CTL run (e.g., Figure 2 at 0000 UTC November 6). The differences in the propagation speed of thunderstorms between the three model runs may be explained by studying the lower tropospheric zonal winds (Figures 6 and 7). The faster zonal winds in the $TOPO_{50\%}$ run helps steer the thunderstorms cells relatively quickly across the Congo basin.

5 | CONCLUDING REMARKS

5.1 | Conclusion

In this study, a large MCS event over equatorial Africa is simulated using WRF at a convection-allowing resolution to investigate the dynamic aspects of perturbing orography. Given the poor representation of orography in GCMs (Figure 1), the purpose of this study is to fill an

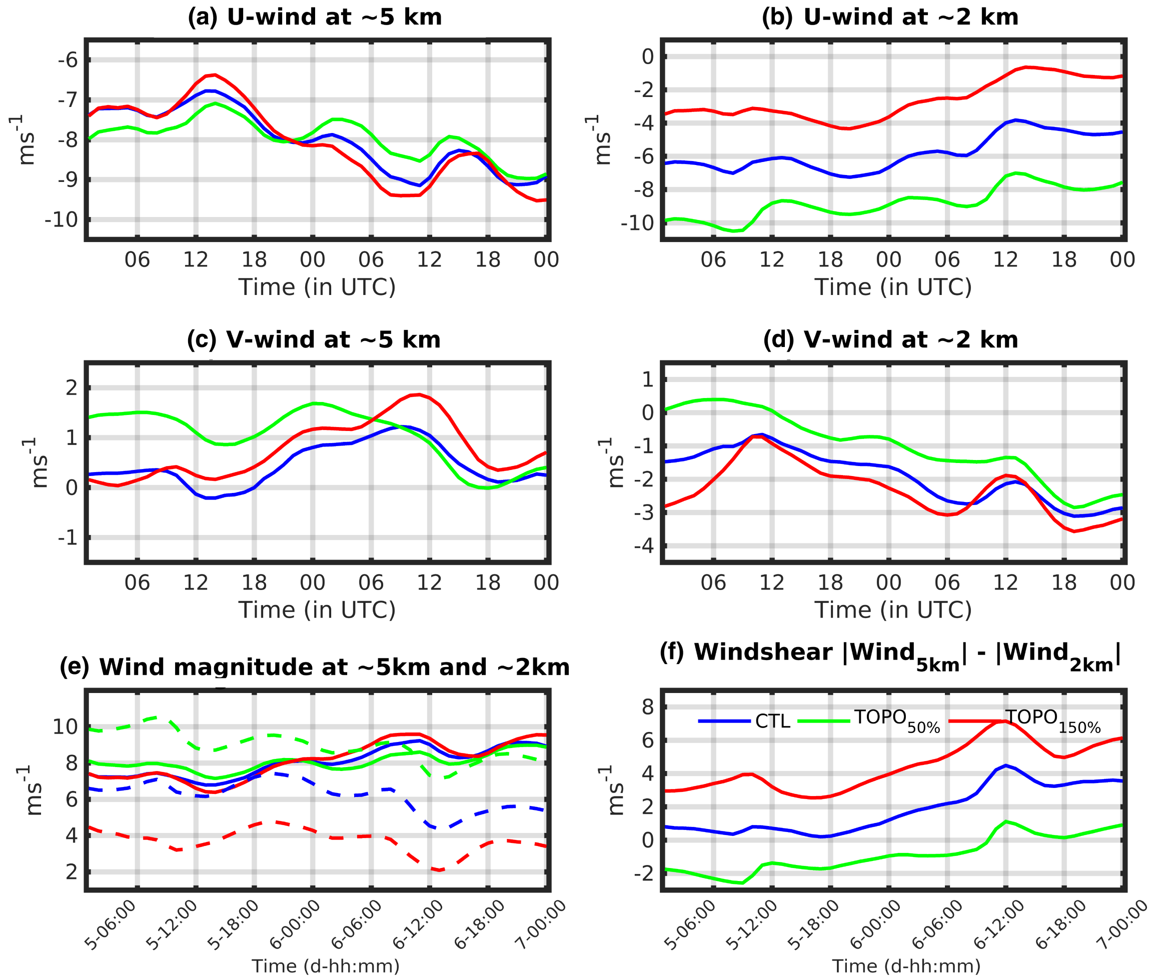

FIGURE 7 (a, b) Zonal and (c, d) meridional wind at $\tilde{5}$ and 2 km, (e) wind magnitude at 5 km (solid line) and 2 km (dashed line), and (f) windshear. Data were spatially averaged between 5°N/S and 12–28°E and shown from 0000 UTC on November 5 to 0000 UTC on November 7, 2014

important knowledge gap by highlighting the important relationship between African orography and rainfall over the Congo basin. While the complex orographic features surrounding the Congo basin have been suggested to play some role in modulating thunderstorms and rainfall (Jackson *et al*., 2009), the physical mechanisms have not been previously investigated. This work provides a dynamic assessment of orography, and the overall results complement previous studies such as Slingo *et al*. (2005), Jackson *et al*. (2009), and Sommerfeld *et al*. (2016). The dynamical impact of the African orography includes blocking of the tropical easterlies, which increasing the vertical windshear. The increase in lower-level wind convergence in an already moist tropical environment may enhance the low-level moisture flux convergence, which is an important ingredient for thunderstorm activity (Cloutier-Bisbee *et al*., 2019). In summary, the dynamical impact of raising the orography of the East African highlands in this case study is a weakening of the lower-tropospheric zonal wind, that results in (1) an increase in the vertical wind shear producing well-sheared and intense MCSs, (2) slower propagation speed for the MCSs, and (3) rainfall enhancement over the Congo Basin.

5.2 | Possible future study

The Congo basin acts as a catchment zone, and the complex orography and vegetation distribution making up the Congo basin (Runge, 2007; Alsdorf *et al*., 2016) results in substantial differences between the Congo river basin (watershed) and the Congo rainforest. The watershed is larger and includes nine riparian countries, including the relatively arid southern Congo basin. The rainforest on the other hand refers to the region that encompasses the

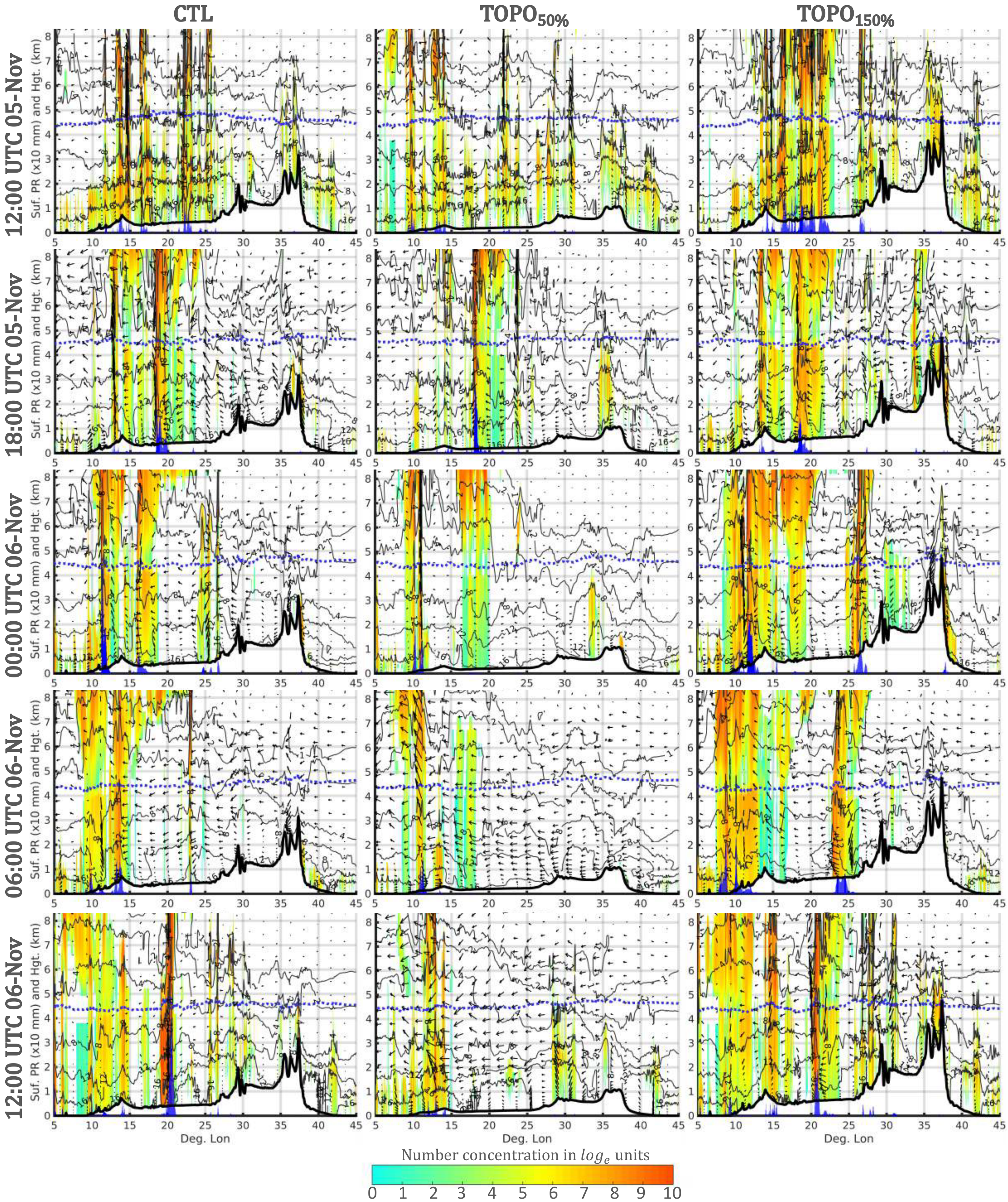

FIGURE 8 Longitude-height cross section along the equator showing the rain/ice particle number concentration (shaded), specific humidity (g kg^{-1}; gray contour), zonal and vertical wind (×10) vector (ms^{-1}), the freezing level (dotted blue line), and rainfall (×10 mm; blue bars along the *x*-axis) for the CTL, TOPO$_{50\%}$, and TOPO$_{150\%}$ runs

humid tropical region with higher rainfall amount (Runge, 2007; Alsdorf *et al*., 2016). Therefore, the spatial distribution of rainfall plays an important role in determining the hydrology (e.g., water table, soil moisture, and run off) and ecology of the Congo basin. Therefore, investigating the complex relationship between the spatial distribution of thunderstorm activity, rainfall and vegetation could potentially lead to a better understanding of the observed long-term drying trend and future of the Congo rainforest. These hydrological properties of the Congo basin could be further investigated by using models such as WRF-Hydro® (Gochis *et al*., 2020).

Finally, improving the horizontal resolution and the representation of orography in GCMs (Dai, 2006; Chen & Dai, 2019), or incorporating high-resolution regional climate models (e.g., Future Climate for Africa FCFA, Improving Model Processes for African Climate - IMPALA project; Stratton *et al*., 2018) will significantly improve our understanding of the hydrological cycle and reduce uncertainties of future climate projections over the Congo. Future study may include the statistical and composite analysis using the IMPALA data to identify mechanisms (e.g., low-level jet, thermodynamic stability, and windshear) responsible for high and low convective events for each season for both the present and future climates. Changes linked to perturbing orography also result in microphysical changes such as the orographic seeder–feeder mechanism (Wilson & Barros, 2014) which act to enhance rainfall could be analyzed in future studies. Finally, improving the horizontal resolution and the representation of orography in GCMs (Dai, 2006; Chen & Dai, 2019), or using high-resolution regional climate models (e.g., CP4-Africa data from the IMPALA project; Stratton *et al*., 2018) could significantly improve our understanding of the hydrological cycle and reduce uncertainties of future climate projections over the Congo. The CP4-Africa could be used to identify mechanisms (e.g., low-level jet, thermodynamic stability, and windshear) responsible for generating intense MCS's in each season for both present and future climates.

ACKNOWLEDGMENTS

This work is supported by the National Science Foundation (NSF AGS-1535426 and AGS-1854486). Geng Xia's effort is supported by the National Renewable Energy Laboratory, operated by Alliance for Sustainable Energy, LLC, for the U.S. Department of Energy (DOE) under Contract No. DE-AC36-08GO28308. Funding was provided by the U.S. Department of Energy Office of Energy Efficiency and Renewable Energy Wind Energy Technologies Office. All datasets used in this study are free and publicly available: The ERA-I dataset is available from the ECMWF website ecmwf.int, The GridSat-B1 data may be accessed from NOAA NCEI THREDDS Data Server (ncei.noaa.gov/thredds/satellite/gridsat_b1.html), and the IMERG data may be accessed from NASA's website doi.org/10.5067/GPM/IMERG/3B-HH/06. Satellite images for this case study are available from the GIBBS archive ncdc.noaa.gov/gibbs/html/MSG-3/IR/2014-11-05-00. The constructive comments from two anonymous reviewers significantly improved this manuscript.

AUTHOR CONTRIBUTIONS

Ajay Raghavendra: Conceptualization; data curation; formal analysis; investigation; methodology; resources; software; validation; visualization; writing – original draft; writing – review and editing. **Geng Xia:** Conceptualization; methodology; resources; software; writing – review and editing. **Liming Zhou:** Conceptualization; formal analysis; funding acquisition; investigation; methodology; project administration; resources; supervision; writing – review and editing. **Yan Jiang:** Conceptualization; data curation; investigation; resources; writing – review and editing.

ORCID

Ajay Raghavendra https://orcid.org/0000-0002-1707-6963

REFERENCES

Alsdorf, D., Beighley, E., Laraque, A., Lee, H., Tshimanga, R., O'Loughlin, F. et al. (2016) Opportunities for hydrologic research in The Congo Basin. *Reviews of Geophysics*, 54, 378–409.

Chen, D. & Dai, A. (2019) Precipitation characteristics in the community atmosphere model and their dependence on model physics and resolution. *Journal of Advances in Modeling Earth Systems*, 11, 2352–2374.

Chen, F. & Dudhia, J. (2001) Coupling an advanced landsurface hydrology model with the Penn State/NCAR MM5 modeling system. Part I: model description and implementation. *Monthly Weather Review*, 129, 569–585.

Chen, Q., Fan, J., Hagos, S., Gustafson, W.I., Jr. & Berg, L.K. (2015) Roles of wind shear at different vertical levels: cloud system organization and properties. *Journal of Geophysical Research – Atmospheres*, 120, 6551–6574.

Cloutier-Bisbee, S.R., Raghavendra, A. & Milrad, S.M. (2019) Heat waves in Florida: climatology, trends, and related precipitation events. *Journal of Applied Meteorology and Climatology*, 58, 447–466.

Crowhurst, D., Dadson, S., Peng, J. & Washington, R. (2021) Contrasting controls on Congo Basin evaporation at the two rainfall peaks. *Climate Dynamics*, 56, 1609–1624.

Dai, A. (2006) Precipitation characteristics in eighteen coupled climate models. *Journal of Climate*, 19, 4605–4630.

Dee, D.P., Uppala, S.M., Simmons, A.J., Berrisford, P., Poli, P., Kobayashi, S. et al. (2011) The ERA-interim reanalysis: configuration and performance of the data assimilation system. *Quarterly Journal of Royal Meteorological Society*, 137, 553–597.

Dudhia, J. (1989) Numerical study of convection observed during the winter monsoon experiment using a mesoscale twodimensional model. *Journal of the Atmospheric Sciences*, 46, 3077–3107.

Dyer, E.L.E., Jones, D.B.A., Nusbaumer, J., Li, H., Collins, O., Vettoretti, G. et al. (2017) Congo Basin precipitation: assessing seasonality, regional interactions, and sources of moisture. *Journal of Geophysical Research – Atmospheres*, 122, 6882–6898.

Gochis, D.J., Barlage, M., Cabell, R., Casali, M., Dugger, A., FitzGerald, K., McAllister, M., McCreight, J., RafieeiNasab, A., Read, L., Sampson, K., Yates, D. & Zhang, Y. (2020). The WRF-hydro® modeling system technical description, (version 5.1.1). NCAR Technical Note. pp. 107.

Haensler, A Saeed, F Jacob, D 2013 Assessment of projected climate change signals over Central Africa based on a multitude of global and regional climate projections. In: Haensler, A., Jacob, D., Kabat, P. & Ludwig, F. (Eds.) *Climate change scenarios for The Congo Basin*. Hamburg, Germany: Climate Service Centre Report No. 11. ISSN: 2192-4058.

Hong, S.-Y., Noh, Y. & Dudhia, J. (2006) A new vertical diffusion package with an explicit treatment of entrainment processes. *Monthly Weather Review*, 134, 2318–2341.

Huffman, G.J Bolvin, D.T Nelkin, E.J Tan, J 2019a Integrated Multi-satellitE Retrievals for GPM (IMERG) Technical Documentation. NASA GSFC. pp. 77.

Huffman, G.J. Stocker, E.F. Bolvin, D.T. Nelkin, E.J. Tan, J. 2019b GPM IMERG Final Precipitation L3 Half Hourly 0.1 degree x 0.1 degree V06, Greenbelt, MD, Goddard Earth Sciences Data and Information Services Center (GES DISC), doi: https://doi.org/10.5067/GPM/IMERG/3B-HH/06[Accessed 23rd June 2020].

Jackson, B., Nicholson, S.E. & Klotter, D. (2009) Mesoscale convective systems over western equatorial Africa and their relationship to large-scale circulation. *Monthly Weather Review*, 137, 1272–1294.

Jiménez, P.A., Dudhia, J., González-Rouco, J.F., Navarro, J., Montávez, J.P. & García-Bustamante, E. (2012) A revised scheme for the WRF surface layer formulation. *Monthly Weather Review*, 140, 898–918.

King, J.A., Engelstaedter, S., Washington, R. & Munday, C. (2021) Variability of the Turkana low-level jet in reanalysis and models: implications for rainfall. *Journal of Geophysical Research – Atmospheres*, 126, e2020JD034154.

Knapp, K.R. (2008) Scientific data stewardship of international satellite cloud climatology project B1 global geostationary observations. *Journal of Applied Remote Sensing*, 2, 023548.

Knapp, K.R., Ansari, S., Bain, C.L., Bourassa, M.A., Dickinson, M.J., Funk, C. et al. (2011) Globally gridded satellite (GridSat) observations for climate studies. *Bulletin of the American Meteorological Society*, 92, 893–907.

Laing, A.G., Carbone, R.E. & Levizzani, V. (2011) Cycles and propagation of deep convection over equatorial Africa. *Monthly Weather Review*, 139, 2832–2853.

Malhi, Y., Adu-Bredu, S., Asare, R.A., Lewis, S.L. & Mayaux, P. (2013) African rainforests: past, present and future. *Philosophical Transactions of the Royal Society B*, 368, 20120312.

Marion, G.R. & Trapp, R.J. (2019) The dynamical coupling of convective updrafts, downdrafts, and cold pools in simulated supercell thunderstorms. *Journal of Geophysical Research – Atmospheres*, 124, 664–683.

Mlawer, E.J., Taubnam, S.J., Brown, P.D., Iacono, M.J. & Clough, S.A. (1997) Radiative transfer for inhomogeneous atmospheres: RRTM, a validated correlated-k model for the longwave. *Journal of Geophysical Research*, 102, 16663–16682.

Motzer, T. (2005) Micrometeorological aspects of a tropical mountain forest. *Agricultural and Forest Meteorology*, 135, 230–240.

Munday, C., Washington, R. & Hart, N. (2021) African low-level jets and their importance for water vapor transport and rainfall. *Geophysical Research Letters*, 48, e2020GL090999.

Pontoppidan, M., Kolstad, E.W., Sobolowski, S.P., Sorteberg, A., Liu, C. & Rasmussen, R.M. (2019) Large-scale regional model biases in the extratropical North Atlantic storm track and impacts on downstream precipitation. *Quarterly Journal of Royal Meteorological Society*, 145, 2718–2732.

Raghavendra, A., Zhou, L., Jiang, Y. & Hua, W. (2018) Increasing extent and intensity of thunderstorms observed over The Congo Basin from 1982 to 2016. *Atmospheric Research*, 213, 17–26.

Rasmussen, K.L. & Houze, R.A., Jr. (2016) Convective initiation near the Andes in subtropical South America. *Monthly Weather Review*, 144, 2351–2374.

Runge, J. (2007) The Congo River, Central Africa, Chap. 14. In: Gupta, A. (Ed.) *Large Rivers: Geomorphology and Management*. Chichester, UK: Wiley, pp. 293–309.

Skamarock, W.C., Klemp, J.B., Dudhia, J., Gill, D.O., Barker, D., Duda, M.G., Huang, X., Wang, W. & Powers, J.G. (2008). A description of the Advanced Research WRF version 3. NCAR Tech. Note NCAR/TN-475+STR. pp. 113. https://doi.org/10.5065/D68S4MVH.

Slingo, J., Spencer, H., Hoskins, B., Berrisford, P. & Black, E. (2005) The meteorology of the western Indian Ocean, and the influence of the east African highlands. *Philosophical Transactions of the Royal Society London A*, 363, 25–42.

Sommerfeld, A., Prömmel, K. & Cubasch, U. (2016) The east African rift system and the impact of orographic changes on regional climate and the resulting aridification. *International Journal of Earth Sciences*, 105, 1779–1794.

Sorí, R., Nieto, R., Vicente-Serrano, S.M., Drumond, A. & Gimeno, L. (2017) A Lagrangian perspective of the hydrological cycle in The Congo River basin. *Earth System Dynamics*, 8, 653–675.

Sotillo, M.G., Ramis, C., Romero, R., Alonso, S. & Homar, V. (2003) Role of orography in the spatial distribution of precipitation over the Spanish Mediterranean zone. *Climate Research*, 23, 247–261.

Stratton, R.A., Senior, C.A., Vosper, S.B., Folwell, S.S., Boutle, I.A., Earnshaw, P.D. et al. (2018) A pan-African convection-permitting regional climate simulation with the met Office unified model: CP4-Africa. *Journal of Climate*, 31, 3485–3508.

Taylor, C.M., Fink, A.H., Klein, C., Parker, D.J., Guichard, F., Harris, P.P. et al. (2018) Earlier seasonal onset of intense mesoscale convective Systems in The Congo Basin since 1999. *Geophysical Research Letters*, 45, 13458–13467.

Taylor, K.E., Stouffer, R.J. & Meehl, G.A. (2012) An overview of CMIP5 and the experiment design. *Bulletin of the American Meteorological Society*, 93, 485–498.

Thompson, G., Field, P.R., Rasmussen, R.M. & Hall, W.D. (2008) Explicit forecasts of winter precipitation using an improved bulk microphysics scheme. Part II: implementation of a new snow parameterization. *Monthly Weather Review*, 136, 5095–5115.

Washington, R., James, R., Pearce, H., Pokam, W.M. & Moufouma-Okia, W. (2013) Congo Basin rainfall climatology: can we believe the climate models? *Philosophical Transactions of the Royal Society B*, 368, 20120296.

Wei, H.-H. & Bordoni, S. (2016) On the role of the African topography in the south Asian monsoon. *Journal of the Atmospheric Sciences*, 73, 3197–3212.

Wilson, A.M. & Barros, A.P. (2014) An investigation of warm rainfall microphysics in the southern Appalachians: orographic enhancement via low-level seeder–feeder interactions. *Journal of the Atmospheric Sciences*, 71, 1783–1805.

Zhou, L., Tian, Y., Myneni, R.B., Ciais, P., Saatchi, S., Liu, Y.Y. et al. (2014) Widespread decline of Congo rainforest greenness in the past decade. *Nature*, 509, 86–90.

How to cite this article: Raghavendra, A., Xia, G., Zhou, L., & Jiang, Y. (2022). Orographic enhancement of rainfall over the Congo Basin. *Atmospheric Science Letters*, *23*(4), e1079. https://doi.org/10.1002/asl.1079